Drug Design, Development and Therapy

Dovepress
Taylor & Francis Group

Open Access Full Text Article

ORIGINAL RESEARCH

Vaccarin Ameliorates Renal Fibrosis by Inhibiting Ferroptosis via Nrf2/SLC7A11/GPX4 Signaling Pathway

Mengjiao Cui[1,2,*], Qiming Xu[1,2,*], Lianxiang Duan[1], Jianrao Lu[1], Jing Hu[1]

[1]Department of Nephropathy, The Seventh People's Hospital, Shanghai University of Traditional Chinese Medicine, Shanghai, 200137, People's Republic of China; [2]Shanghai University of Traditional Chinese Medicine, Shanghai, 201203, People's Republic of China

*These authors contributed equally to this work

Correspondence: Jing Hu; Jianrao Lu, Department of Nephropathy, The Seventh People's Hospital, Shanghai University of Traditional Chinese Medicine, Shanghai, People's Republic of China, Email 6264570@qq.com; jianraolu@163.com

Purpose: Vaccarin is a natural flavonoid glycoside with anti-inflammatory, antioxidant and nephroprotective effects. However, the effects of vaccarin on renal fibrosis (RF) and its molecular mechanisms remain unclear. This study aimed to investigate the effects of vaccarin on RF and its molecular mechanisms.

Methods: Network pharmacology was used to analyze the effect of vaccarin on RF, and molecular docking and molecular dynamics simulations were performed to assess the binding of nuclear factor erythroid 2-related factor 2 (Nrf2) to vaccarin. A mouse model of unilateral ureteral obstruction (UUO) was established in vivo, and human renal tubular epithelial (HK2) cells were induced with transforming growth factor-β (TGF-β) and RSL3, respectively, as an in vitro model. The anti-fibrotic effect of vaccarin was observed by histopathological staining and determination of fibrous markers. Changes in oxidative stress and ferroptosis-related markers were detected by kits, Western blot (WB), qRT-PCR and immunofluorescence (IF). Finally, Nrf2 inhibitors were added to the in vitro model to observe the effects on fibrosis and ferroptosis.

Results: Vaccarin and RF cross genes are enriched for oxidative stress. Nrf2 binds stably to vaccarin. Both in vivo and in vitro experiments showed that vaccarin treatment reduced the expression of fibrosis markers, decreased the levels of reactive oxygen species (ROS), malondialdehyde (MDA), lipid peroxidation (LPO) and Fe^{2+}, and increased glutathione (GSH) secretion. In addition, vaccarin down-regulated the expression of Long-chain acyl-CoA synthetase 4 (ACSL4), prostaglandin-endoperoxide synthase 2 (PTGS2) and NADPH oxidase 1 (NOX1), and up-regulated Nrf2 and its downstream solute transport family 7 member 11 (SLC7A11) and glutathione peroxidase 4 (GPX4) expression. Mechanistic studies indicated that vaccarin activated the Nrf2/SLC7A11/GPX4 pathway to inhibit ferroptosis, and this inhibition was effectively reversed by the Nrf2 inhibitor.

Conclusion: Vaccarin ameliorates RF by inhibiting ferroptosis via Nrf2/SLC7A11/GPX4 pathway.

Keywords: vaccarin, renal fibrosis, Nrf2/SLC7A11/GPX4 pathway, ferroptosis, oxidative stress, network pharmacology

Introduction

Chronic kidney disease (CKD) is a significant global public health issue, affecting more than 10% of the global population,[1] with its prevalence continuing to rise annually.[2,3] RF characterized by tubulointerstitial fibrosis and progression to end-stage renal disease, is a common pathological feature of various forms of CKD.[4] Sustained inflammation and oxidative stress can induce renal tubular injury accompanied by the release of large amounts of inflammatory factors that promote fibroblast proliferation and extracellular matrix deposition, thereby accelerating the process of RF.[5,6] However, the precise pathogenesis remains poorly understood. Thus, there is an urgent need to find effective treatments to improve RF.

Studies have shown that oxidative stress and disturbances in iron metabolism can lead to renal ferroptosis.[7–9] Ferroptosis, a form of iron-dependent cell death distinct from apoptosis and autophagy, is characterized by oxidative

Received: 4 December 2024
Accepted: 28 February 2025
Published: 6 March 2025

stress and the accumulation of lipid ROS.[10,11] In the kidney, excessive Fe^{2+} levels may participate in the Fenton reaction, leading to lipid peroxidation and ROS production.[12] Nrf2 is a key regulator of the cellular antioxidant response, protecting cells from oxidative stress, inflammation and various growth factors.[13] Under basal conditions, Nrf2 levels are tightly regulated and subject to degradation by the E3 ubiquitin ligase complex. However, during oxidative stress, ROS interact with Kelch-like ECH-associated protein 1 (Keap1), leading to the dissociation of Nrf2 from Keap1, its stabilization, and subsequent nuclear translocation. This process activates the expression of downstream antioxidant genes.[14,15] SLC7A11 and GPX4 are critical antioxidant proteins that inhibit ferroptosis by reducing lipid peroxide formation,[10,16] both SLC7A11 and GPX4 are regulated by Nrf2.[17] Recent studies have shown that ferroptosis inducers exacerbate renal injury and RF in CKD models, while inhibitors of ferroptosis can mitigate renal damage and fibrosis.[18] Therefore, identifying novel ferroptosis inhibitors holds significant potential for the treatment of RF.

Vaccarin, a natural flavonoid glycoside found in the seeds of *Vaccaria hispanica*, possesses well-documented anti-inflammatory and antioxidant properties.[19–21] Previous studies have demonstrated that vaccarin mitigates oxidative stress and reduces apoptosis and necrosis in a cisplatin-induced acute kidney injury model.[22] Additionally, vaccarin has been shown to improve renal function and alleviate renal tissue damage in diabetic mice by inhibiting RF, inflammatory factors, and ROS production.[23] These findings suggest a promising therapeutic potential for vaccarin in the treatment of kidney diseases. However, to date, no studies have investigated the protective effects of vaccarin against RF or explored its molecular mechanisms in the context of RF treatment.

In the present study, we employed network pharmacology to identify the therapeutic targets of vaccarin in RF and assessed its therapeutic potential using in vivo and in vitro models of RF. Furthermore, we investigated the molecular mechanisms underlying its effects, with particular emphasis on the relationship between vaccarin and ferroptosis. The results of this study can inform further research on the improvement of RF by vaccarin.

Materials and Methods

Acquisition of Structural Formulae and Targets of Vaccarin

Information about vaccarin and its 2D and 3D structural formulae were obtained from the PubChem public database (https://pubchem.ncbi.nlm.nih.gov/) using "Vaccarin" as the keyword, which was subsequently imported into the SwissTargetPrediction database (https://swisstargetprediction.ch/), the Similarity ensemble approach database and Netlnfer database (http://lmmd.ecust.edu.cn/netinfer/) to find potential targets can be found, and a large amount of literature was searched for complementary information.

Analysis of Vaccarin Related Targets

Establishment of gene interaction network by UniProt database (https://www.uniprot.org/) and STRING database (https://cn.string-db.org/). An "active compound-target" PPI networks were constructed using Cytoscape 3.9.1 software to observe the relationship between vaccarin and potential targets.

Collection of Targets of RF Action by Vaccarin

We utilized the GSE20247 dataset from the GEO database (https://www.ncbi.nlm.nih.gov/geo/) to investigate the gene expression profiles associated with human chronic kidney disease. This dataset comprises microarray data from 18 samples, focusing on genes related to renal tubular epithelial cell injury. The selected gene expression data was further analyzed using the GEO2R analytical tool. Obtaining RF-related targets from GeneCards (https://www.genecards.org/), OMIM (https://www.omim.org/), MALACARDS (https://www.malacards.org/) and DisGeNET (https://ngdc.cncb.ac.cn/databasecommons/database/) databases and presented in a Venn diagram.

Analysis of Overlapping Genes

PPI data were extracted using the STRING database and then imported into Cytoscape 3.7.2 software, followed by a screening of core genes using the CentiScape 2.2 algorithm.

GO and KEGG Pathway Enrichment Analysis

Using the Metascape database (https://metascape.org/gp/index.html), we performed GO and KEGG analysis of the differential and visualized them with the ggplot2 package in R4.2.1.

Molecular Docking and Molecular Dynamics Simulation

The 3D structural model of the Nrf2 protein was obtained from the UniProt database, and the ligand file of vaccarin in SDF format was obtained from the PubChem database. The docking results were further analyzed and visualized using Discovery Studio 2019 software. Molecular dynamics simulations with the GROMACS 2022 program provide insight into the stability of protein-ligand interactions. The hydrogen bonds involved were constrained using the LINCS algorithm with an integration step of 2 fs. The electrostatic interactions were calculated using the Particle mesh Ewald method with a cutoff of 1.2 nm and a cutoff of 10 Å for non-bonding interactions, updated every 10 steps. The simulated temperature was 298 K and the pressure was 1 bar. Simulated trajectories were analyzed with VMD and pymol.

Reagents

Vaccarin (AB0659, purity 98%) was purchased from ABPHYTO (Chengdu, China). The Losartan tablets were obtained from MSD (Hangzhou, China). TGF-β (AF-100-21C-100) was obtained from Pepro Tech (America). RSL3 (S8155), Ferrostatin-1 (Fer-1, S7243) and ML385 (S8790) were purchased from Selleck (Shanghai, China).

UUO Induced Animal Model

C57BL/6 mice (SPF-grade, male, 7-week-old, weighing 18–22 g) provided by the Jihui Laboratory Animal Care Co., Ltd (Shanghai, China). The mice were kept in the Central Laboratory of the Seventh People's Hospital. All operations in this study followed the guidelines for laboratory animals, and the protocol was approved by the Ethics Committee of Shanghai Seventh People's Hospital (approval number: 2024-AR-017). In addition, in terms of the care of laboratory animals, we strictly abide by the Guiding Principles of Laboratory Animal Welfare and Ethics issued by the Ministry of Science and Technology of the People's Republic of China.

After adaptation for 1 week, thirty mice were randomly assigned to five groups (sham group, UUO group, 12.5 mg/kg vaccarin treatment group, 25 mg/kg vaccarin treatment group and 8.57 mg/kg Losartan positive control group, 6 mice per group). Mice were anesthetized with pentobarbital sodium, and a longitudinal incision was made on the left side of the abdomen to expose the left ureter, which was double ligated with a 4–0 silk suture, and then the incision was closed. The mice in the sham group were operated identically except that the ureter was not ligated. Subsequently, mice in vaccarin-treated and Losartan groups were gavaged for 14 days with the corresponding concentration of the drug, and mice in sham and UUO groups were gavaged with an equal volume of saline. At the end of treatment, the mice were euthanized, and serum and kidney tissues were removed for subsequent experiments.

Cell Culture

The HK2 cell was obtained from Shanghai Cell Bank, Chinese Academy of Sciences. Cells were grown in DMEM/F-12 medium containing 6% FBS at 37°C with 5% CO_2. HK2 cells were inoculated into 6-well plates and cultured overnight. The next day, the medium was changed to a medium containing 0.5% FBS with TGF-β, RSL3, Fer-1, ML385 or vaccarin for 48 h.

Hematoxylin-Eosin (HE) and Masson Staining

Kidney tissues were paraffin-embedded and cut into sections of 4 μm thickness. Staining was performed according to HE (D006-1-1, Jiancheng, Nanjing, China) and Masson (D026-1-3, Jiancheng, Nanjing, China) instructions. Images are presented by Leica SCN400 Slide Scanning System and software. Renal tubular injury was assessed in a double-blind manner and scored according to the severity of the injury.[24] Collagen deposition was also scored in a double-blind analysis.

Prussian Blue Staining

Paraffin sections of kidney tissue were stained according to the instructions of the Prussian blue (60533ES20, YEASEN, Shanghai, China) kit. Images are presented by Leica SCN400 Slide Scanning System and software.

WB Assays

Protein was extracted from kidney tissues and HK2 cells by adding protease inhibitors (ST506, Beyotime, Shanghai, China) with RIPA lysate (P0013B, Beyotime, Shanghai, China). Samples containing 25 μg of protein were separated on 7.5% gel and transferred to a PVDF membrane (Millipore, ISEQ00010), followed by 5% milk and incubation with antibodies against Fibronectin (1:2500, ab45688, Abcam, USA), N-Cadherin (1:500, sc-8424, Santa Cruz), p-Smad3 (1:2000, ET1609-41, HUABIO), Smad3 (1:1000, ET1607-41, HUABIO), α-SMA (1:2000, ET1607-53, HUABIO), Snail (1:2000, A11794, ABclonal), Nrf2 (1:1000, 16396-1-AP, proteintech), SLC7A11 (1:2000, HA600098, HUABIO), GPX4 (1:10000, ET1706-45, HUABIO), Keap1 (1:1000, D6B12, Cell Signaling), GAPDH (1:5000, 60004-1-Ig, proteintech), Lamin B1 (1:2000, ET1606-27, HUABIO) and β-actin (1:2000, AC004, ABclonal) overnight at 4°C. After three TBST washes, the PVDF membrane was incubated with the secondary antibody (1:10000, HA1001 and HA1006, HUABIO) for 1 h at room temperature. Luminescence detection was performed with the ECL system and analyzed by Image J software.

qRT-PCR

Total RNA was extracted from kidney tissue using a kit (R401-01, Vazyme, China). qRT-PCR analysis was performed with the StepOne Plus Sequence Detection System. The final analysis was performed using the $2^{-\Delta\Delta CT}$ relative quantification method. The primer sequences used are shown in Table 1.

IF Staining

HK2 cells were inoculated in 12-well culture dishes containing slides and intervened with different concentrations of vaccarin for 24 h. Kidney tissue paraffin and HK2 cells were stained according to the instructions of the Three-color Fluorescence Kit (RC0086-23RM, Recordbio Biological Technology, Shanghai, China). Finally, the image was presented with a Leica DMi8 fluorescence microscope.

GSH, MDA and LPO Assays

Mouse blood samples were centrifuged at room temperature, 3000 rpm for 15 min and the upper serum layer was removed. GSH and MDA levels in mouse serum and HK2 cells were measured with the GSH and MDA (A006-2-1, A003-1, Jiancheng, Nanjing, China) kit. LPO level in kidney tissue and HK2 cells were measured with the LPO (A106-1-2, Jiancheng, Nanjing, China) kit.

Table 1 Primer Sequences

Gene	Forward Primer (5′-3′)	Reverse Primer (5′-3′)
m-SLC7A11	CTTTGTTGCCCTCTCCTGCTTC	CAGAGGAGTGTGCTTGTGGACA
m-GPX4	CCTCTGCTGCAAGAGCCTCCC	CTTATCCAGGCAGACCATGTGC
m-Nrf2	TCTCCTCGCTGGAAAAAGAA	AATGTGCTGGCTGTGCTTTA
m-ACSL4	GGAAAGCAAACTGAAGGCGG	AATGGCCATGTCTGAAGGGG
m-PTGS2	TGAGCAACTATTCCAAACCAGC	GCACGTAGTCTTCGATCACTATC
m-NOX1	AGAGAGACAGGTGCCTTTGC	GCTGCATGACCAGCAATGTT
m-Fibronectin	CCCTATCTCTAGTACCGTTGTCC	TGCCGCAACTACTGTGATTCGG
m-Snail	AAGATGCACATCCGAAGC	ATCTCTTCACATCCGAGTGG
m-GAPDH	GGTTGTCTCCTGCGACTTCA	TGGTCCAGGGTTTCTTACTCC

Fe^{2+} Assays

The levels of Fe^{2+} in kidney tissue were measured with the Fe^{2+} (A039-2-1, Jiancheng, Nanjing, China) kit. Fe^{2+} levels in HK2 cells were detected with FerroOrange (F374, Dojindo Laboratories, Japan) and fluorescence intensity with Image J.

Detection of ROS

ROS levels in HK2 cells were determined with the ROS (S0033S, Beyotime, Shanghai, China) kit.

Cell Viability

HK2 cells were inoculated in 96-well culture plates and cultured overnight. The cells interfered with vaccarin, TGF-β, RSL3, and Fer-1 for 24h. Cell viability was assessed according to the CCK-8 (40203ES, YEASEN, Shanghai, China) kit.

Statistical Analysis

Statistical analysis and bar graphs were performed using GraphPad Prism software. Data are expressed as mean ± SD. Differences between multiple groups were compared using one-way ANOVA. $P < 0.05$ indicated statistically significant differences.

Results

Prediction and Analysis of the Action Targets of Vaccarin

Firstly, the basic information and molecular structural formula of vaccarin were obtained from the PubChem database (Figure 1A). Subsequently, 197 target genes of vaccarin were identified from SwissTargetPrediction, Similarity ensemble approach and Netlnfer databases. A network of 153 nodes and 1272 edges was constructed by obtaining the network data from the STRING database and visualizing it with the Cytoscape 3.9.1 software (Figure 1B). Analysis of the targets revealed that the 197 target genes were mainly enriched in amino acid metabolism (Figure 1C). KEGG analysis suggested that 197 genes were mainly enriched in PI3K-Akt signaling pathway, Human T-cell leukemia virus 1 infection, Cellular senescence, MAPK signaling pathway, Cell cycle, Measles, Hepatitis B, Ras signaling pathway, JAK-STAT signaling pathway (Figure 1D). It is well known that amino acids can be involved in the regulation of RF by affecting multiple signaling pathways. The above analysis suggests that vaccarin has the potential to treat RF.

Analysis of Potential Targets of Vaccarin on RF

We analyzed the mechanism of action of vaccarin on RF using a web-based pharmacological system. A total of 5525 DEGs were obtained from the GSE20247 dataset, and the volcano map (Figure 2A) was plotted with "Adjusted P < 0.05 and log2 (fold change) > 1 or log2 (fold change) < −1" as the initial screening condition. A total of 6399 RF-associated targets were obtained by merging the above genes with GeneCards, OMIM, MALACARDS and DisGeNET databases and removing duplicate values. The targets associated with vaccarin and RF were further analyzed using a Wayne diagram, and a total of 70 potential targets were obtained and analyzed for protein interactions (Figure 2B). The above genes were then imported into the STRING database, and after eliminating the irrelevant genes, the PPI network was constructed using Cytoscape 3.9.1 software. As shown in Figure 2C, the "vaccarin target-RF target" network was constructed in the left graph, in which the yellow nodes were 35 crossed genes. The middle figure is the network diagram of 35 crossover genes, and the yellow nodes of these 35 genes (which may be the more important genes) were obtained by setting parameters (Betweenness>204.1, Closeness>0.527, Degree>16.3). The right figure shows the core genes obtained according to the algorithm of degree value, including AKT1, IL-6, TNF, BCL2, EGFR and so on. The validation results of the above genes are supplemented in Supplementary Material 1. Enrichment analysis of the above core genes revealed that changes in biological processes are closely linked to oxidative stress (Figure 2D). KEGG pathways enrichment analysis revealed that PI3K-Akt signaling pathway, JAK-STAT signaling pathway, AGE-RAGE signaling pathway in diabetic complications and other related signaling pathways (Figure 2E). We believe that vaccarin action on RF is closely related to oxidative stress.

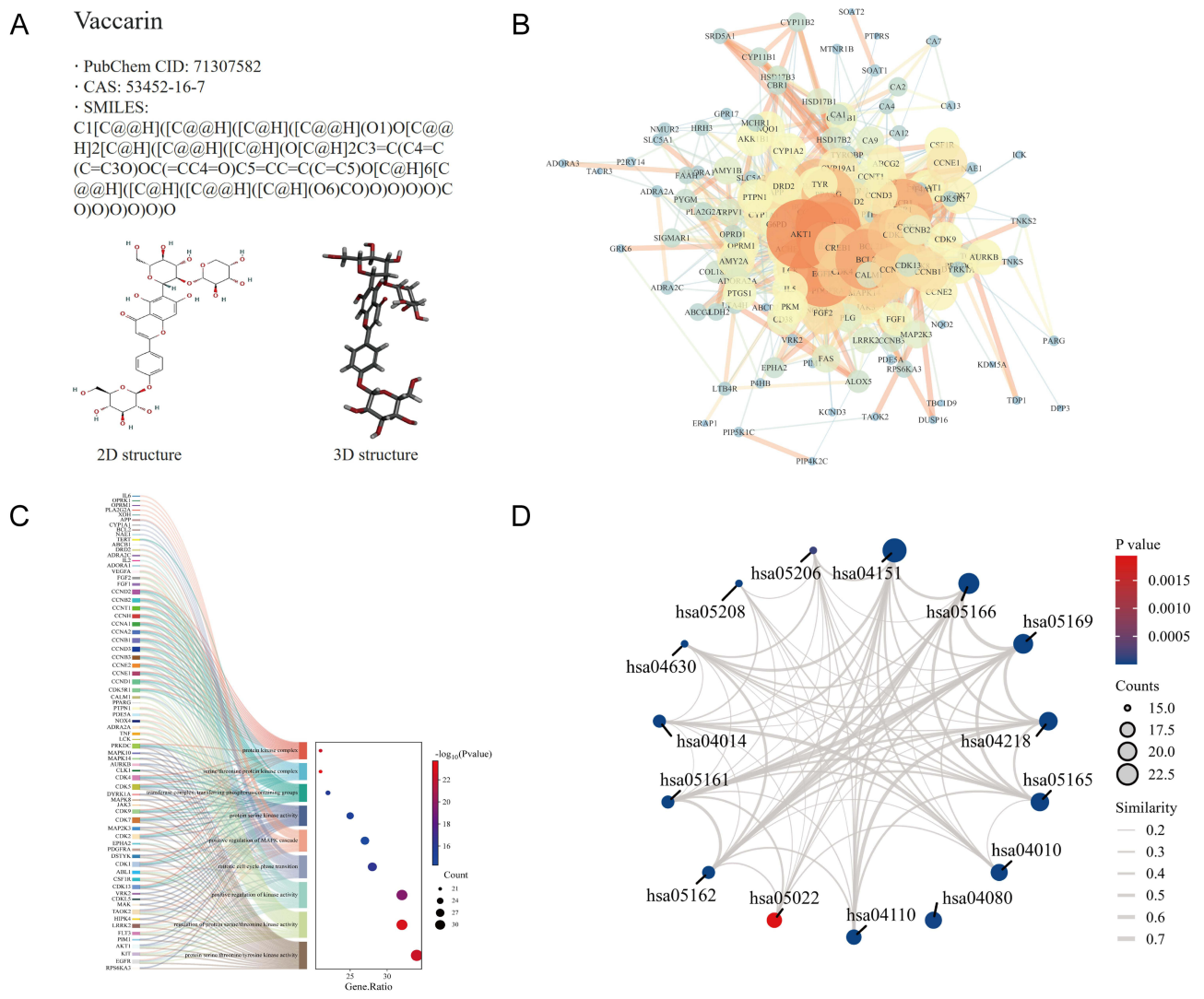

Figure 1 Prediction and analysis of vaccarin targets. (**A**) 2D and 3D structures and related information of vaccarin. (**B**) "Compound-target" network consisting of 153 nodes and 1272 edges. (**C**) Sankey diagram of vaccarin target genes and the corresponding enrichment process. (**D**) String diagram of KEGG signaling pathway of vaccarin target genes.

Vaccarin Binds Stably to Nrf2

Nrf2 is an important transcription factor regulating oxidative stress, it has been reported that some flavonoids can exert antioxidant effects by modulating Nrf2. Here, we assessed the binding ability of vaccarin to Nrf2 by Molecular Docking and Molecular Dynamics simulation. The Molecular Docking results showed that vaccarin had good binding to Nrf2 (Figure 3A). To further verify the binding ability between vaccarin and Nrf2, we performed a Molecular Dynamics simulation. Firstly, we performed stability analysis, Root Mean Square Deviation (RMSD) is a common measure of the difference between two structures, reflecting the similarity of the conformation of the two molecules, the RMSD of the complex structure, and the RMSD of the proteins were gradually stabilized as a whole as the simulation progressed (Figure 3B). Radius of Gyration (Rg) is an important parameter for measuring the overall structural compactness of a protein-small molecule, reflecting the range of distribution of molecular atoms with respect to the centre of mass, the Rg of the complexes remained essentially stable as the simulation proceeded (Figure 3C). Root mean square fluctuation (RMSF) can be used to measure the magnitude of the displacement of each atom or residue with respect to its average position, which can help to identify the flexible and rigid regions in the molecules (Figure 3D). The state of the small molecule on the protein surface can be clarified by the centre-of-mass evolution analysis, the distance between the small

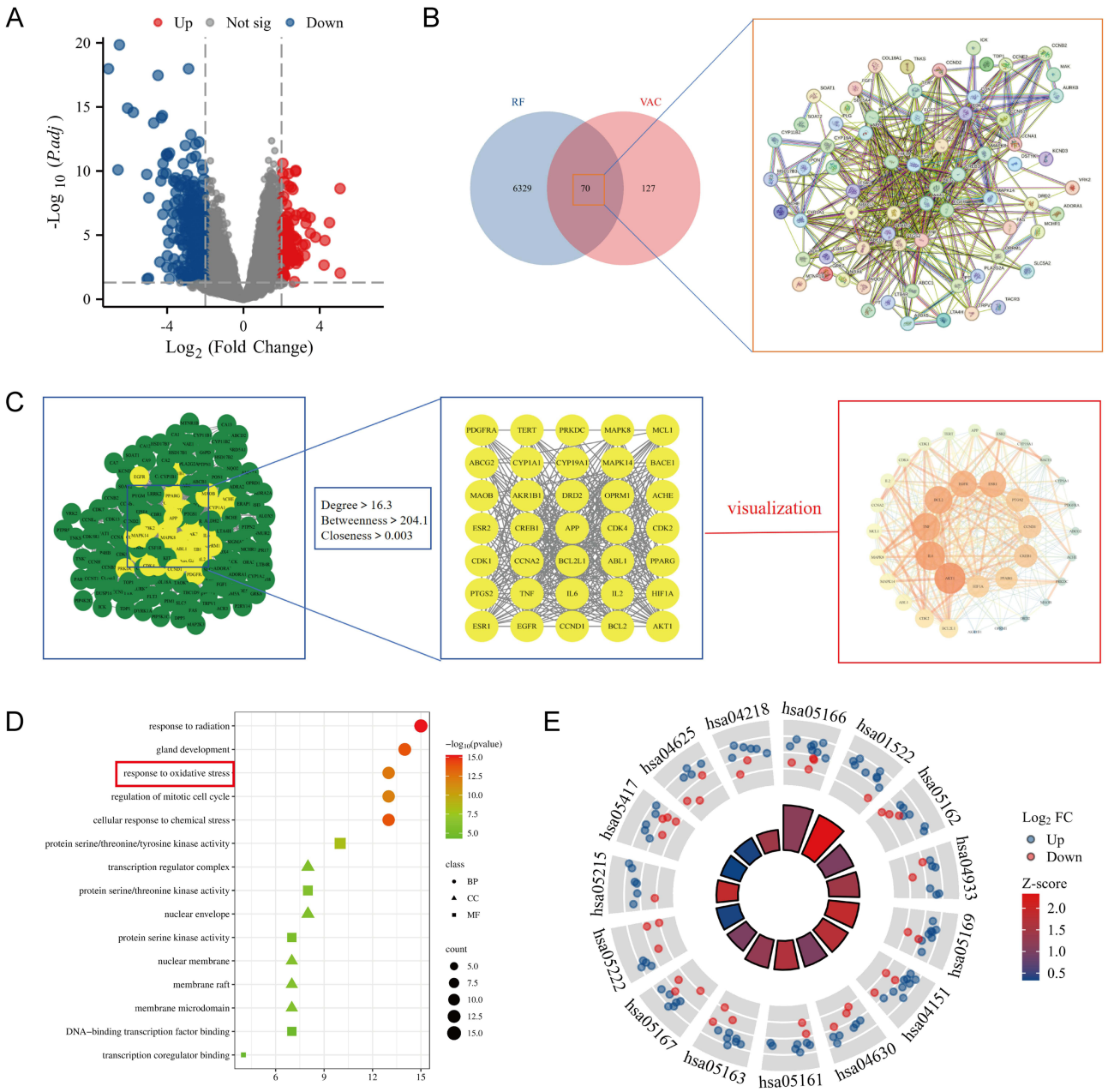

Figure 2 Screening and analysis of potential targets of RF by vaccarin. (**A**) Differential gene volcano plot for RF. Blue represents up-regulation, red represents down-regulation, and grey indicates no statistical difference. (**B**) Venn diagram of interactions between vaccarin targets and RF targets. (**C**) Target gene network diagram. The "vaccarin target-RF" network constructed by 70 crossover genes and 35 key genes obtained by three algorithms, Betweenness, Closeness, and Degree. (**D**) Bubble map of GO enrichment analysis. (**E**) Circle diagram of KEGG enrichment analysis.

molecule and the initial binding site is gradually stabilized, indicating that vaccarin is stably bound to the initial Nrf2 binding site (Figure 3E). Buried Solvent Accessible Surface Area (BuriedSASA) is used to assess which parts of a molecule or molecular complex are buried internally and cannot be directly accessed by the solvent, the Buried SASA is gradually stabilized, suggesting that the area of contact between vaccarin and Nrf2 remains stable (Figure 3F). Secondly, we analyzed the interaction of hydrogen bonding between vaccarin and Nrf2. Hydrogen bonding interaction is an important force for protein-ligand binding, the number of hydrogen bonds between vaccarin and Nrf2 mainly remains fluctuating between 3–7 (Figure 3G). Finally, we calculated the change in force upon binding of vaccarin to Nrf2. VDW is more stable relative to ELE in the complex, and both VDW and ELE are stable (Figure 3H). These results indicate that the binding between vaccarin and Nrf2 is stable.

https://doi.org/10.2147/DDDT.S509357

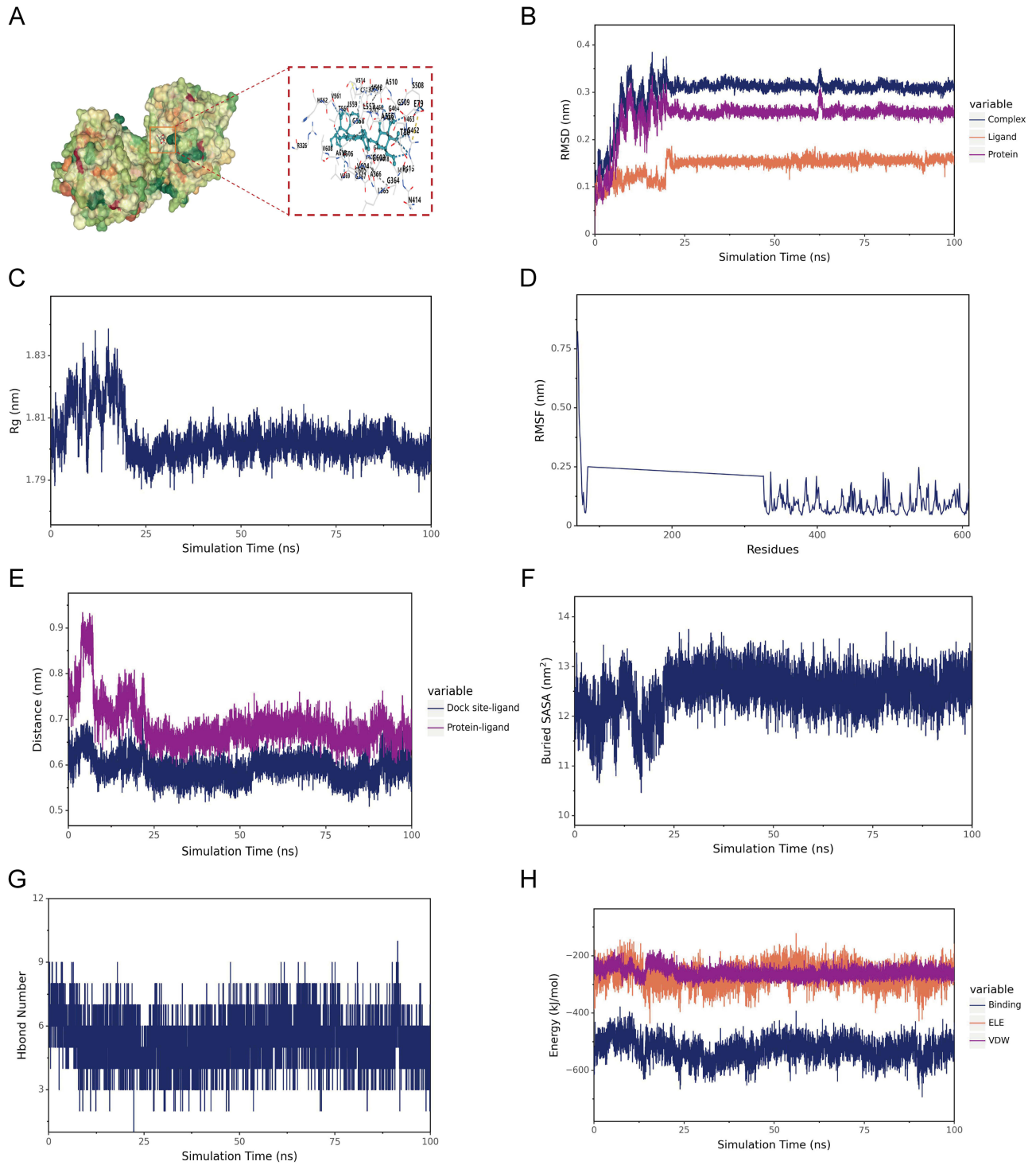

Figure 3 Molecular docking and molecular dynamics simulations of vaccarin and Nrf2 proteins. (**A**) Molecular docking diagram of Nrf2 with vaccarin. (**B**) RMSD of Nrf2, vaccarin ligand, and the complex. (**C**) Rg of Nrf2 in complex with vaccarin. (**D**) RMSF of the protein in the Nrf2-vaccarin complex. (**E**) Spacing of the Nrf2-vaccarin binding site (Dock site-ligand). (**F**) Encapsulation area between vaccarin and Nrf2 protein (Buried SASA). (**G**) Hydrogen bond number (Hbond number). (**H**) Binding energy between vaccarin and Nrf2 protein (VDW and ELE).

Vaccarin Ameliorated RF in UUO Mice

Network pharmacological analysis showed that vaccarin has therapeutic potential for RF. We established a UUO mouse model for in vivo experimental validation. HE and Masson staining were used to assess renal tubular injury and

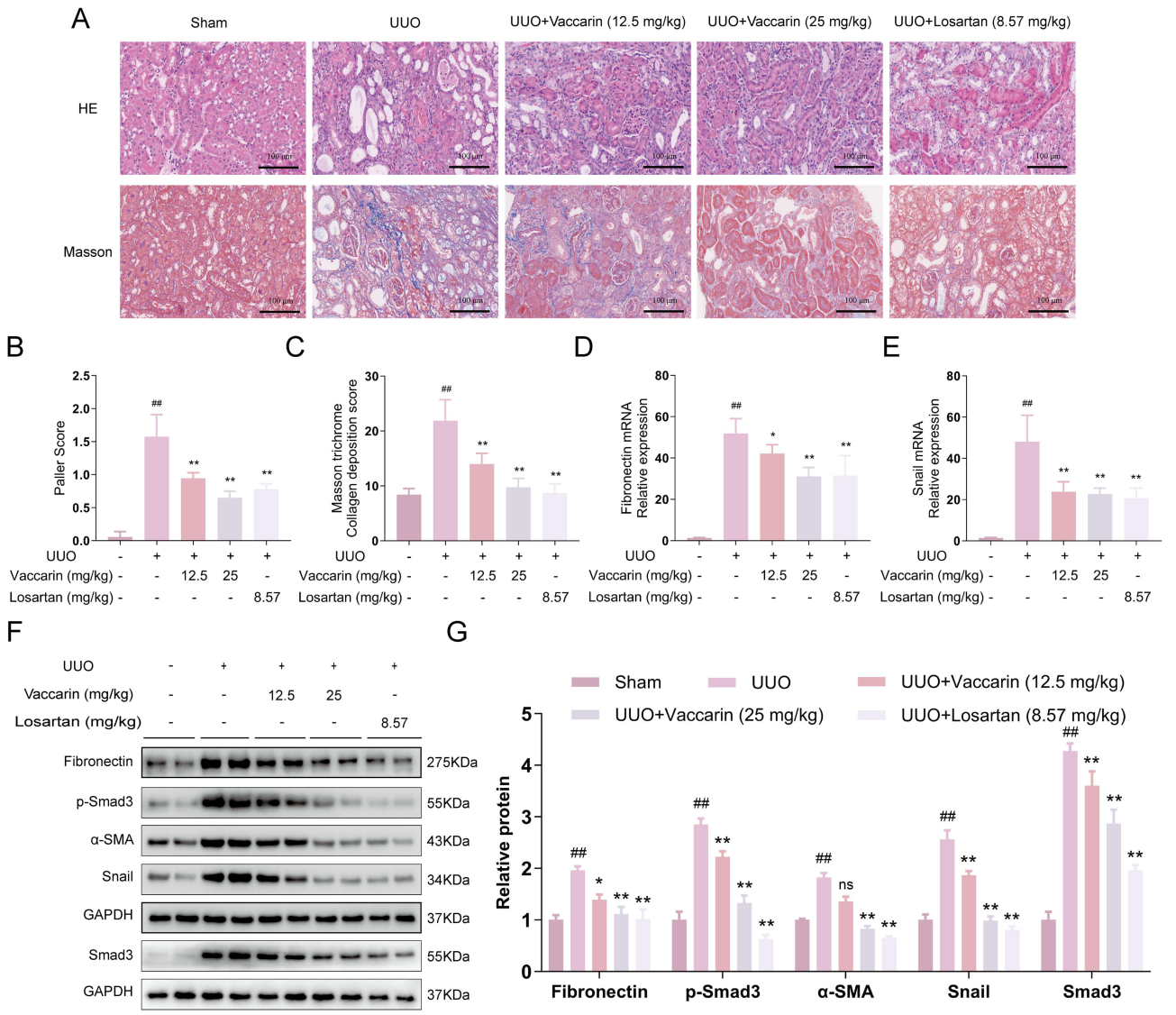

Figure 4 Vaccarin alleviated renal fibrosis in UUO mice. (**A**) HE staining of mouse tissue sections demonstrated degree of renal injury. Renal fibrosis was assessed by Masson's trichrome staining. (Magnification×200, Bar = 100 μm). The quantitative analysis result of HE staining (**B**) and Masson staining (**C**). Levels of Fibronectin (**D**) and Snail (**E**) mRNA in UUO mice. (**F**) The expressions of Fibronectin, p-Smad3, α-SMA, Snail and Smad3 by WB. (**G**) The quantitative analysis of Fibronectin, p-Smad3, α-SMA, Snail and Smad3 by WB. Data are presented as the means ± SD (n = 6). $^{\#\#}P < 0.01$, vs Sham group; $^{*}P < 0.05$, $^{**}P < 0.01$, vs UUO group; ns: $P > 0.05$, no significance.

interstitial fibrosis. Compared with the Sham group, the renal tubules in the UUO group were significantly dilated, and the interstitium had a large infiltration of inflammatory cells and obvious blue collagen deposition. Renal tubular injury and interstitial fibrosis were significantly reduced after vaccarin treatment (Figure 4A–C). Next, qRT-PCR analysis showed that the relative mRNA expression of Fibronectin (FN) and Snail was significantly upregulated in the UUO group, whereas vaccarin treatment underregulated mRNA expression (Figure 4D and E). In addition, WB results indicated the treatment with both doses of vaccarin reduced the expression of FN, phosphorylated Smad3 (p-Smad3), α-smooth muscle actin (α-SMA), Snail and Smad3 (Figure 4F and G). These results suggest that vaccarin attenuates UUO-induced renal tubular injury and fibrosis.

Vaccarin Inhibited Ferroptosis in UUO Mice

Network pharmacological analyses suggest that the rich biological processes of vaccarin are closely related to oxidative stress. To clarify whether vaccarin could enhance the antioxidant capacity of UUO mice, we measured MDA and GSH levels in serum and LPO levels in renal tissues of mice. In the UUO group, MDA and LPO levels were elevated and GSH

https://doi.org/10.2147/DDDT.S509357

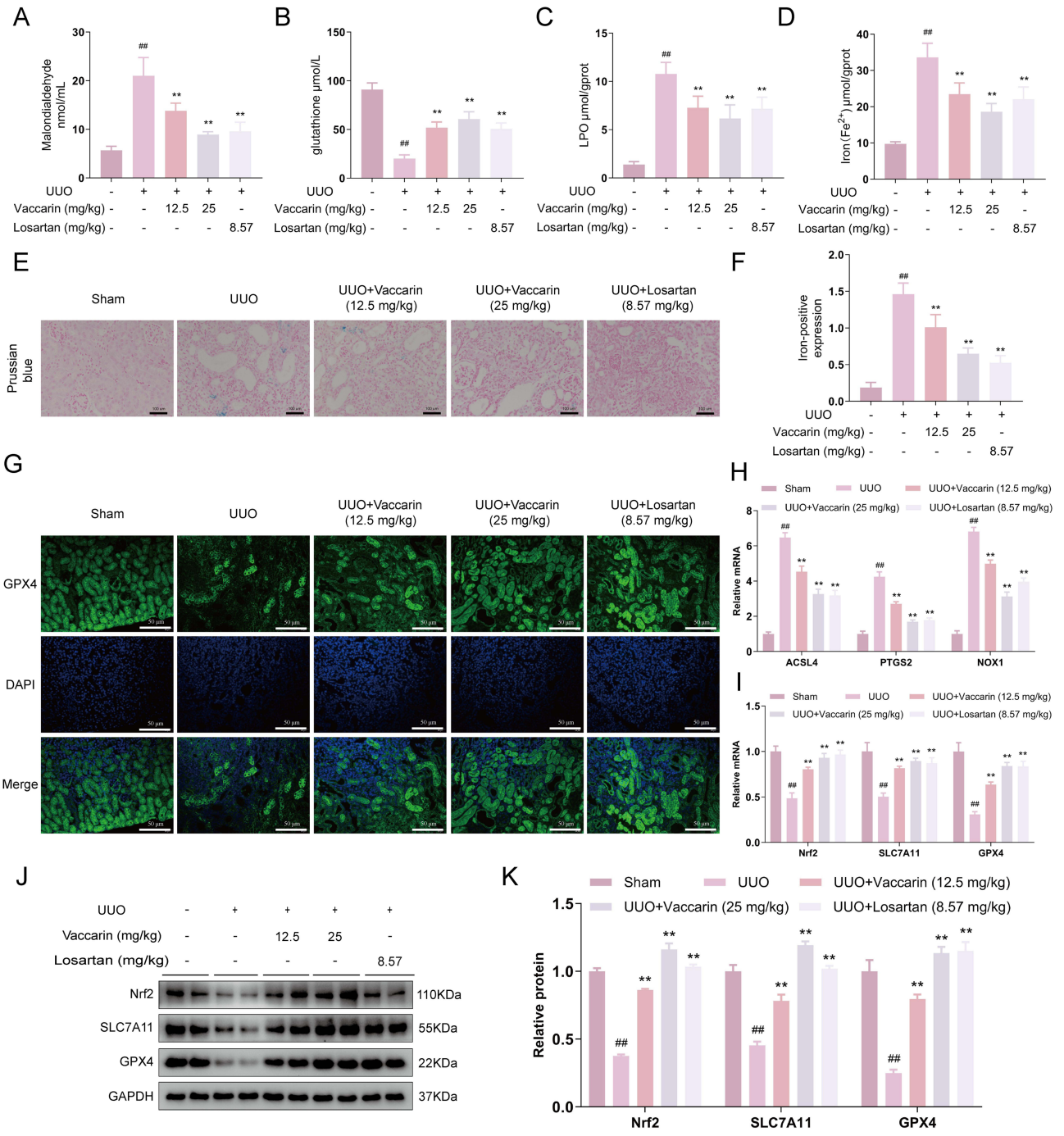

Figure 5 Vaccarin inhibited oxidative stress-induced ferroptosis in UUO mice. (**A**) Serum MDA level. (**B**) Serum GSH level. (**C**) LPO level in renal tissues. (**D**) Fe^{2+} level in renal tissues. (**E** and **F**) Representative images of iron deposition by Prussian blue staining and its quantitative analysis (Magnification×200, Bar = 50 μm). (**G**) Representative images of kidney GPX4 IF staining (Magnification×200, Bar = 50 μm). (**H**) Levels of ACSL4, PTGS2 and NOX1 mRNA in renal tissues. (**I**) Levels of Nrf2, SLC7A11 and GPX4 mRNA in renal tissues. (**J**) The expressions of Nrf2, SLC7A11 and GPX4 by WB. (**K**) The quantitative analysis of Nrf2, SLC7A11 and GPX4 by WB. Data are presented as the means ± SD (n = 6). $^{\#\#}P < 0.01$, vs Sham group, $^{**}P < 0.01$, vs UUO group.

levels were decreased, whereas vaccarin treatment significantly decreased MDA and LPO levels and increased GSH levels (Figure 5A–C). Meanwhile, we also found that Fe^{2+} levels were significantly elevated in renal tissues of UUO group, whereas vaccarin treatment reduced Fe^{2+} levels (Figure 5D). Prussian blue staining also observed iron deposition in kidney tissue of UUO mice, which was attenuated by vaccarin treatment (Figure 5E and F). It has been established that

elevated levels of oxidative stress are a major trigger of ferroptosis, and the pathogenesis of CKD, including RF, is closely related to ferroptosis.[25,26]

The above findings motivate us to further explore the role of ferroptosis in the improvement of RF by vaccarin. From the results of IF staining, it was easy to see that GPX4 was lowly expressed in the UUO group and highly expressed in the vaccarin-treated group (Figure 5G). ACSL4, PTGS2 and NOX1 were highly expressed in the UUO group, and mRNA levels were significantly reduced after vaccarin intervention (Figure 5H). Subsequently, we assessed changes in mRNA and protein levels of two key regulators, SLC7A11 and GPX4, during ferroptosis.[16] In the UUO group, the mRNA and protein expression levels of SLC7A11 and GPX4 were significantly down-regulated, while vaccarin up-regulated their expression in a dose-dependent manner. Nrf2 is essential in regulating SLC7A11 and GPX4 to inhibit ferroptosis.[17] We found that mRNA and protein levels of Nrf2 were significantly lower in the UUO group and significantly higher after vaccarin treatment (Figure 5I–K). The results of in vivo experiments showed that vaccarin could attenuate oxidative stress and ferroptosis in UUO mice by up-regulating Nrf2 and its downstream SLC7A11 and GPX4 expression.

Vaccarin Inhibited TGF-β- and RSL3-Induced Fibrosis in HK2 Cells

To further validate the anti-fibrotic effect of vaccarin, we established an in vitro model with TGF-β-induced HK2 cells. First, we evaluated the cytotoxicity of vaccarin. We found that vaccarin at 7.5, 15, 30, and 60 μM had no significant effect on HK2 cell viability (Figure 6A). RSL3 is a common agonist of ferroptosis.[27] We intervened HK2 cells with TGF-β and RSL3 and assayed cell viability, respectively, and showed that both TGF-β and RSL3 inhibited cell viability, whereas cell viability was increased with either vaccarin or Fer-1 (Figure 6B and C). WB results showed the increased expression of FN, N-Cadherin, α-SMA, Snail and p-Smad3/Smad3 in HK2 cells incubated with TGF-β. Vaccarin significantly decreased the expression of fibrotic markers (Figure 6D and E). Meanwhile, we found that RSL3 intervention in HK2 cells increased the expression of the above fibrotic markers, whereas vaccarin and Fer-1 reversed the increase in fibrotic markers (Figure 6F and G). These findings further confirm the role of ferroptosis in RF, and that vaccarin can significantly ameliorate TGF-β- and RSL3-induced fibrosis.

Vaccarin Inhibited TGF-β- and RSL3-Induced Ferroptosis in HK2 Cells

The ferroptosis process is accompanied by the accumulation of ROS and Fe^{2+}.[28] It has been shown that ferroptosis leads to high production of ROS, promotes oxidative stress and induces renal fibrosis.[8] Elevated levels of Fe^{2+} were observed in HK2 cells induced by TGF-β or RSL3 by FerroOrange probes, whereas both vaccarin and Fer-1 interventions reduced the excessive accumulation of Fe^{2+} (Figure 7A and B). Meanwhile, DCFH-DA probes to detect ROS levels in HK2 cells revealed that TGF-β or RSL3 could induce elevated ROS levels, whereas both vaccarin and Fer-1 interventions reduced ROS expression (Figure 7C and D). Additionally, vaccarin reduced MDA and LPO levels while elevating GSH levels in TGF-β- or RSL3-induced HK2 cells (Figure 7E–G). Similarly, in TGF-β- or RSL3-induced HK2 cells, vaccarin significantly upregulated the expression of Nrf2 and its downstream SLC7A11 and GPX4 (Figure 7H–K). These data suggest that vaccarin can inhibit TGF-β- and RSL3-induced oxidative stress and ferroptosis in HK2 cells by upregulating Nrf2 and its downstream SLC7A11 and GPX4.

Vaccarin Attenuated TGF-β-Induced RF by Promoting Nrf2 Nuclear Translocation

Molecular Docking and Molecular Dynamics simulation revealed that vaccarin binds stably to Nrf2. Studies have shown that flavonoids can exert nephroprotective effects by promoting Nrf2 nuclear translocation.[29] Therefore, we hypothesized that vaccarin may exert antifibrotic effects by promoting Nrf2 nuclear translocation. IF staining showed that vaccarin increased Nrf2 translocation from the cytoplasm to the nucleus (Figure 8A). We subsequently found that vaccarin dose-dependently decreased Nrf2 protein levels in the cytoplasm and increased Nrf2 protein levels in the nucleus by isolating cytoplasmic and nuclear proteins (Figure 8B–D). These results suggest that vaccarin can promote Nrf2 translocation from the cytoplasm to the nucleus. Keap1 is a negative regulator of Nrf2 and plays an important role in regulating oxidative stress responses.[30] We found that when Nrf2 was inhibited by its inhibitor ML385, the upregulation of Nrf2 and its downstream SLC7A11 and GPX4 by vaccarin was significantly suppressed, whereas Keap1 expression was instead

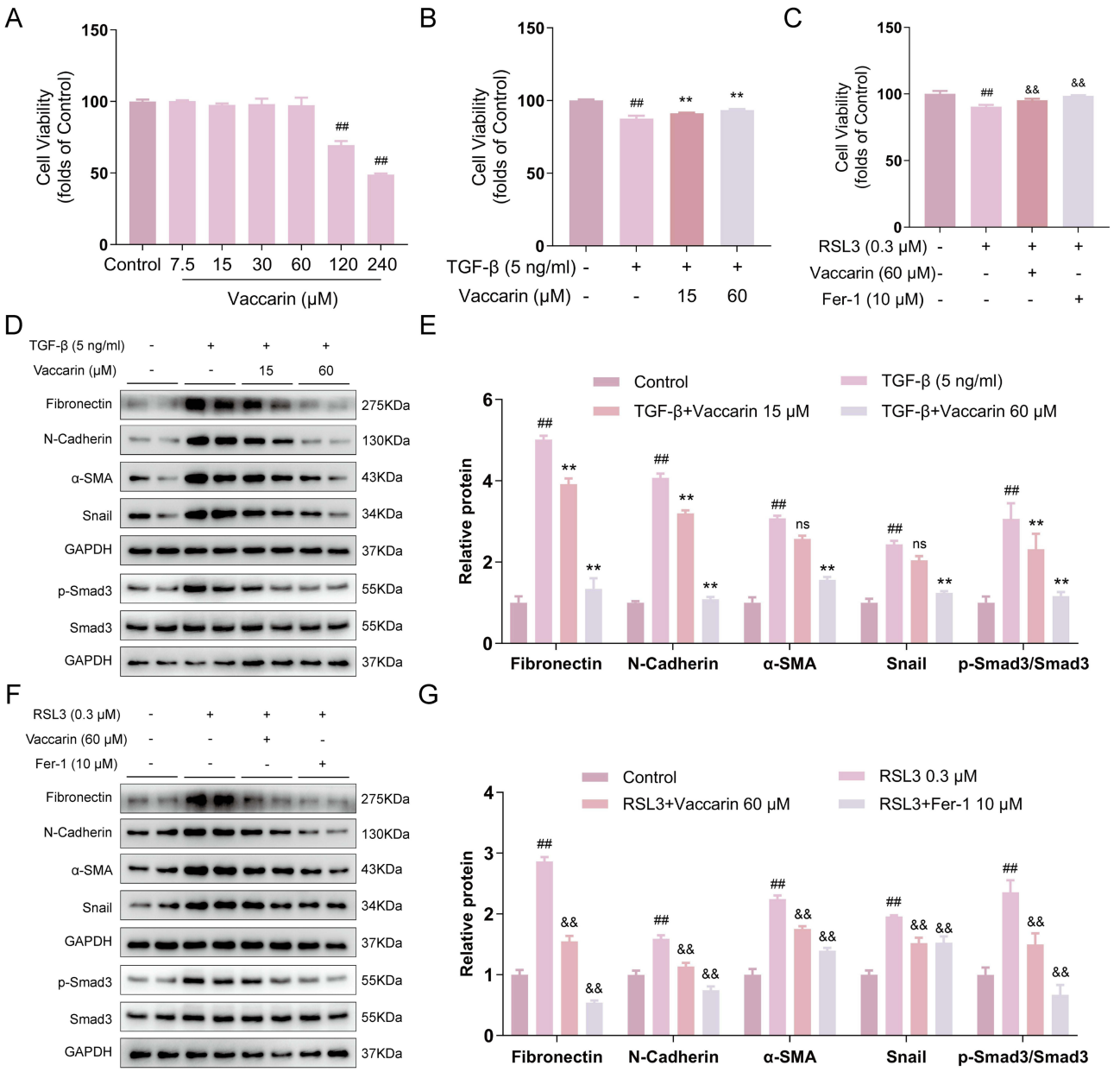

Figure 6 Vaccarin alleviated TGF-β- and RSL3-induced renal fibrosis in HK2 cells. (**A**) Cell Viability in HK2 cells was determined by the CCK-8 assay. (**B** and **C**) CCK-8 assay the impact of vaccarin on TGF-β- and RSL3-induced HK2 cells. (**D**) The expressions of Fibronectin, N-Cadherin, α-SMA, Snail, p-Smad3 and Smad3 by WB in TGF-β-induced HK2 cells. (**E**) The quantitative analysis of Fibronectin, N-Cadherin, α-SMA, Snail and p-Smad3/Smad3 by WB. (**F**) The expressions of Fibronectin, N-Cadherin, α-SMA, Snail, p-Smad3 and Smad3 by WB in RSL3-induced HK2 cells. (**G**) The quantitative analysis of Fibronectin, N-Cadherin, α-SMA, Snail and p-Smad3/Smad3 by WB. Data are presented as the means ± SD (n = 6). $^{\#\#}P < 0.01$, vs Control group; $^{**}P < 0.01$, vs TGF-β group; $^{\&\&}P < 0.01$, vs RSL3 group; ns: $P > 0.05$, no significance.

upregulated (Figure 8E and F). We also found that the antifibrotic effect of vaccarin in TGF-β-induced HK2 cells was significantly reduced when Nrf2 was inhibited (Figure 8G and H). These data suggest that vaccarin inhibits TGF-β-induced HK2 cell fibrosis by disrupting the Keap1-Nrf2 interaction and promoting Nrf2 translocation from the cytoplasm to the nucleus.

Discussion

The pathogenesis of RF is a gradual process involving multiple cytokines and molecular mechanisms, ultimately leading to end-stage renal failure that requires dialysis or renal transplantation.[4] Fibrotic burden serves as a critical indicator of future

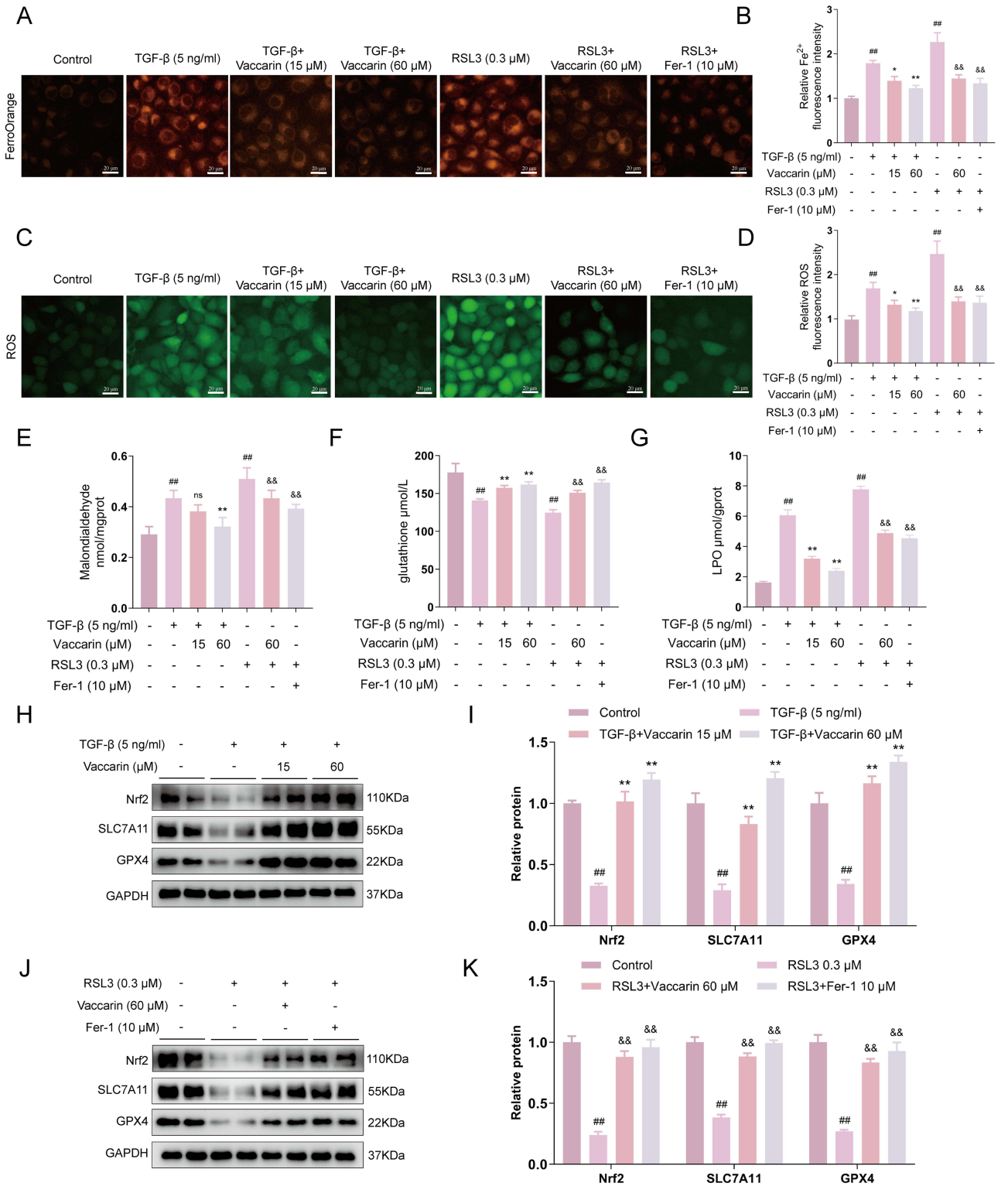

Figure 7 Vaccarin inhibited TGF-β- and RSL3-induced ferroptosis in HK2 cells. (**A** and **B**) FerroOrange probe was used to detect the intracellular Fe^{2+} of cultured HK2 cells (Magnification×200, Bar = 20 μm). (**C** and **D**) Representative images of ROS staining in HK2 cells (Magnification×200, Bar = 20 μm). (**E**) MDA levels in HK2 cells. (**F**) GSH levels in HK2 cells. (**G**) LPO levels in HK2 cells. (**H**) The expressions of Nrf2, SLC7A11 and GPX4 by WB in TGF-β-induced HK2 cells. (**I**) The quantitative analysis of Nrf2, SLC7A11 and GPX4 by WB. (**J**) The expressions of Nrf2, SLC7A11 and GPX4 by WB in RSL3-induced HK2 cells. (**K**) The quantitative analysis of Nrf2, SLC7A11 and GPX4 by WB. Data are presented as the means ± SD (n = 6). $^{\#\#}P < 0.01$, vs Control group; $^{*}P < 0.05$, $^{**}P < 0.01$, vs TGF-β group; $^{\&\&}P < 0.01$, vs RSL3 group; ns: $P > 0.05$, no significance.

https://doi.org/10.2147/DDDT.S509357

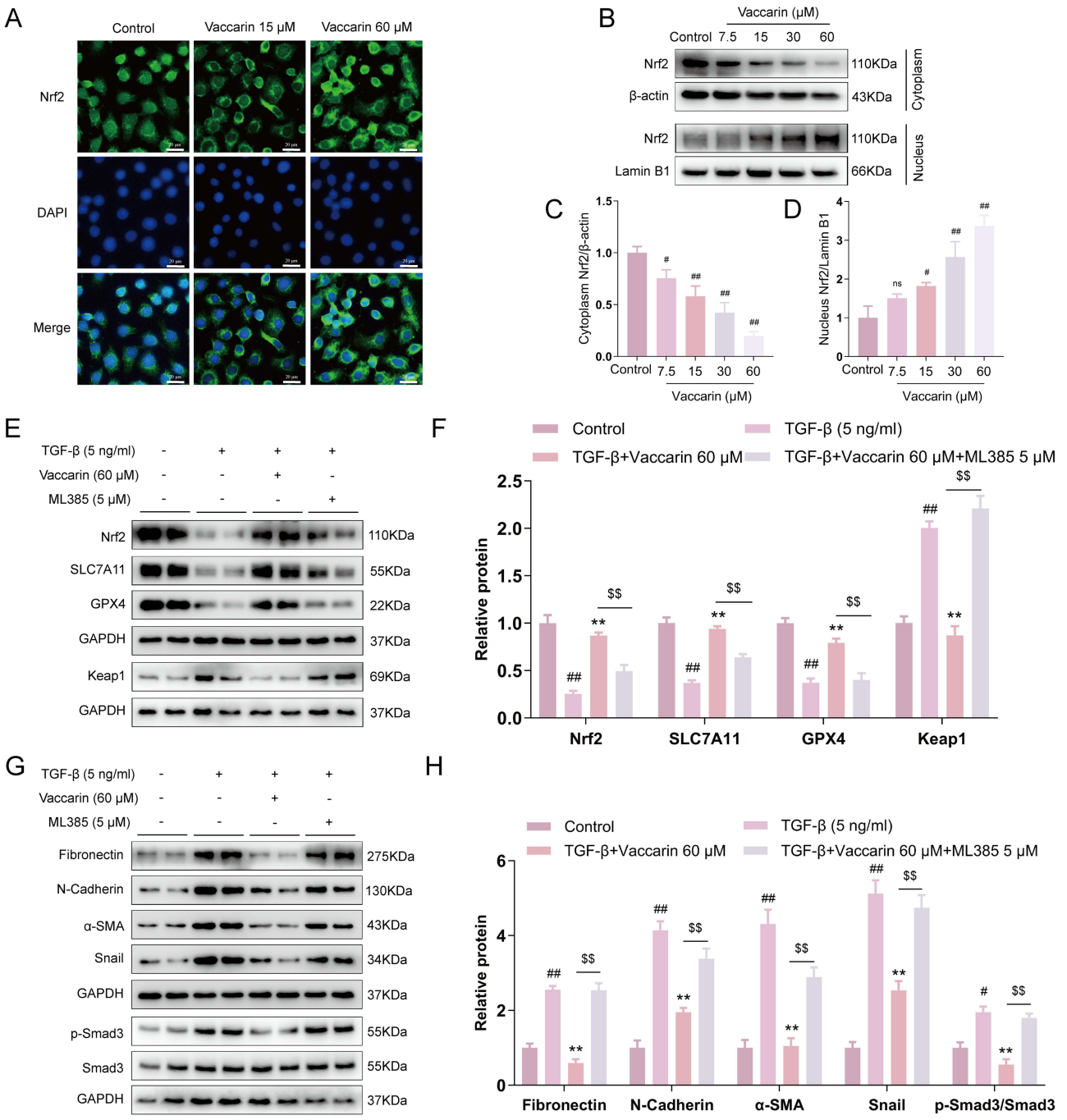

Figure 8 Vaccarin inhibits TGF-β-induced ferroptosis in HK2 cells in an Nrf2 dependent manner. (**A**) IF assay showed the relative abundance of Nrf2 in HK2 cells. (**B**) The levels of Nrf2 protein in Cytoplasm and Nucleus were detected after treatment with different concentrations of vaccarin in HK2 cells. (**C** and **D**) The quantitative analysis of Nrf2 by WB. (**E**) The expressions of Nrf2, SLC7A11, GPX4 and Keap1 by WB in TGF-β-induced HK2 cells. (**F**) The quantitative analysis of Nrf2, SLC7A11, GPX4 and Keap1 by WB. (**G**) The expressions of Fibronectin, N-Cadherin, α-SMA, Snail, p-Smad3 and Smad3 by WB in TGF-β-induced HK2 cells. (**H**) The quantitative analysis of Fibronectin, N-Cadherin, α-SMA, Snail and p-Smad3/Smad3 by WB. Data are presented as the means ± SD (n = 6). $^{\#}P < 0.05$, $^{\#\#}P < 0.01$, vs Control group; $^{**}P < 0.01$, vs TGF-β group; $^{\$\$}P < 0.01$, vs TGF-β+Vaccarin 60 μM group; ns: $P > 0.05$, no significance.

adverse renal outcomes, for which no safe and effective therapies currently exist. This highlights the urgent need for the development of novel therapeutic drugs or treatments. Vaccarin, a natural flavonoid with known anti-inflammatory and antioxidant properties, has shown promising potential for the treatment of kidney disease in previous studies.[31] However, the effects and mechanisms of vaccarin on RF remain unexplored. Network pharmacology offers valuable insights into the molecular mechanisms underlying drug-target-disease interactions. In this study, we found that the therapeutic effect of

vaccarin on RF is closely linked to oxidative stress through network pharmacology. Molecular docking and molecular dynamics simulations suggest that Nrf2 may serve as the specific molecular target through which vaccarin exerts its beneficial effects on RF. In vivo and in vitro experimental studies demonstrated that vaccarin ameliorates fibrosis by inhibiting oxidative stress and ferroptosis through activation of the Nrf2/SLC7A11/GPX4 pathway.

UUO is a commonly used in vivo model to induce RF, which can develop over a relatively short period.[32,33] In the UUO model, the overproduction of ROS triggers inflammation, oxidative stress, and apoptosis, thereby promoting the progression of fibrosis.[34] Losartan, a widely used treatment for CKD-related diseases, has been shown to improve RF.[35] In this study, we investigated the antifibrotic effects of vaccarin using the UUO mouse model, with losartan serving as a positive control. Our findings demonstrate that vaccarin alleviated kidney damage and reduced collagen fiber deposition. We also observed that vaccarin decreased the mRNA expression of FN and snail. Moreover, analysis of RF markers revealed that vaccarin decreased the protein expression of FN, p-Smad3, α-SMA, Snail and Smad3. These findings imply that vaccarin can ameliorate kidney injury and RF in UUO mice. TGF-β is essential for the development of fibrosis and can be used as a target for treatment as well as a gauge of the degree of fibrosis.[36] To investigate vaccarin's antifibrotic properties further, we treated HK2 cells with TGF-β and vaccarin. We found that vaccarin decreased the protein expression of FN, N-Cadherin, p-Smad3/Smad3, α-SMA and Snail in TGF-β stimulated HK2 cells, which is in line with the in vivo results. According to these findings, vaccarin may be able to reduce TGF-β induced fibrosis in HK2 cells in vitro.

The network pharmacology-based target screening of vaccarin for RF, followed by GO enrichment analyses, revealed that its therapeutic effects are closely linked to oxidative stress. Previous studies have found that inhibition of oxidative stress attenuates UUO and TGF-β-induced RF.[37] In this study, we found that vaccarin reduced MDA and LPO levels and increased GSH levels in UUO mice and TGF-β-induced HK2 cells, and also reduced ROS levels in HK2 cells, which confirms the results of the network pharmacology study. Additionally, elevated oxidative factors such as MDA and ROS contribute to ferroptosis during RF.[38] We observed that Fe^{2+} levels were significantly elevated in UUO mice and TGF-β stimulated HK2 cells, which were significantly reduced after vaccarin treatment. SLC7A11 is an amino acid anti-transporter protein that plays a key role in inhibiting ferroptosis by facilitating cystine uptake for GSH synthesis, thereby enhancing the cell's antioxidant capacity.[39] GPX4, a glutathione peroxidase in mammals, prevents ferroptosis by reducing lipid hydroperoxides to lipid alcohols and by inhibiting the accumulation of ROS.[40] Modulation of the SLC7A11/GPX4 pathway to attenuate lipid peroxidation and ferroptosis reduces acute kidney injury.[41] In this study, we observed reduced levels of both SLC7A11 and GPX4 in UUO mice and TGF-β-induced HK2 cells. However, treatment with vaccarin significantly up-regulated the expression of both proteins. Additionally, in HK2 cells induced by ferroptosis agonist RSL3, we detected increased levels of MDA, LPO, ROS and Fe^{2+}, along with decreased expression of GSH, SLC7A11 and GPX4. Notably, treatment with vaccarin and Fer-1 reversed these changes. These findings suggest that vaccarin exerts its anti-renal fibrosis effects by inhibiting oxidative stress and ferroptosis.

Nrf2 is a transcription factor that plays a crucial role in regulating intracellular oxidative stress and exerts antioxidant effects through its translocation to the nucleus.[14] SLC7A11 and GPX4 are key components of the ferroptosis pathway, both of which are modulated by Nrf2. It has been found that pentoxifylline protects against cerebral ischemia-reperfusion injury by inhibiting ferroptosis through the Nrf2/SLC7A11/GPX4 pathway.[42] Keap1 is a negative regulatory protein of Nrf2. Under normal conditions, Nrf2 is degraded in the Keap1-Nrf2 axis, whereas under oxidative stress, Nrf2 dissociates from the Keap1-Nrf2 axis and translocates to the nucleus, where it induces a series of antioxidant responses.[15,43] It has been shown that notoprotein R1 promotes Nrf2 nuclear translocation to inhibit ferroptosis and attenuate myocardial injury through the Keap1/Nrf2 pathway.[44] In this study, molecular docking and molecular dynamics simulations revealed that Nrf2 may be a key target of vaccarin for the alleviation of RF. Based on the interaction between vaccarin and Nrf2, we hypothesized that vaccarin may exert its anti-fibrotic effects by promoting Nrf2 nuclear translocation and inhibiting ferroptosis. Initially, we observed a significant reduction in Nrf2 levels in UUO mice and TGF-β/RSL3 induced HK2 cells, which were elevated after vaccarin treatment. This suggests that the onset of ferroptosis during RF progression may be linked to Nrf2 downregulation. Further investigation using IF and WB confirmed that vaccarin promoted the translocation of Nrf2 from the cytoplasm to the nucleus in a dose-dependent manner. To validate these findings, we utilized ML385, an Nrf2 inhibitor, and observed that the antifibrotic effects of vaccarin, along with the inhibition of ferroptosis, were reversed by ML385. We also found that vaccarin inhibited Keap1 expression, and this

inhibition was subsequently counteracted by ML385. We suggest that vaccarin disrupts the Keap1-Nrf2 interaction and promotes Nrf2 nuclear translocation, thereby exerting an antifibrotic effect. However, the use of ML385 alone may not be sufficient to fully determine the potential of vaccarin on Keap1-Nrf2, and knockdown or overexpression as well as immunoprecipitation experiments are considered in the future for confirmation.

Collectively, our results suggest that vaccarin can improve RF by inhibiting ferroptosis via Nrf2/SLC7A11/GPX4 signaling pathway. Although studies have reported the use of vaccarin in renal injury, its role in RF has not been reported. The present study highlights for the first time the antifibrotic properties of vaccarin, which act by inhibiting ferroptosis through the Nrf2/SLC7A11/GPX4 pathway.

Conclusion

In summary, our study demonstrates that vaccarin can improve RF by activating the Nrf2/SLC7A11/GPX4 signaling pathway and inhibiting ferroptosis. In addition, we confirmed that Nrf2 is a target of vaccarin action. These suggest that vaccarin has the potential to improve RF and warrants further exploration for clinical application.

Abbreviations

RF, renal fibrosis; Nrf2, nuclear factor erythroid 2-related factor 2; UUO, unilateral ureteral obstruction; HK2, human renal tubular epithelial; TGF-β, transforming growth factor-β; WB, Western blot; IF, immunofluorescence; ROS, reactive oxygen species; MDA, malondialdehyde; LPO, lipid peroxidation; GSH, glutathione; ACSL4, Long-chain acyl-CoA synthetase 4; PTGS2, prostaglandin-endoperoxide synthase 2; NOX1, NADPH oxidase 1; SLC7A11, solute carrier family 7 member 11; GPX4, glutathione peroxidase 4; CKD, chronic kidney disease; Keap 1, Kelch-like ECH-associated protein 1; Fer-1, ferrostatin-1; HE, hematoxylin-eosin; RMSD, root mean square deviation; Rg, radius of gyration; RMSF, root mean square fluctuation; BuriedSASA, buried solvent accessible surface area; FN, fibronectin; p-Smad3, phosphorylated Smad3; α-SMA, α-smooth muscle actin.

Ethical Approval

All the databases in this study are public databases whose contents are publicly available and can be reused without restriction through open licenses. According to the official documents issued by the National Science and Technology Ethics Committee of China, the use of legally obtained public databases is not subject to ethical review (https://www.gov.cn/zhengce/zhengceku/2023-02/28/content_5743658.htm). Therefore, the part of this study involving human data from public databases required exemption from ethical approval (Ethics Committee of Shanghai Seventh People's Hospital).

Acknowledgment

We sincerely thank the Central Laboratory of the Seventh People's Hospital affiliated to Shanghai University of Traditional Chinese Medicine for its great support and the reviewers of the paper for their guidance.

Author Contributions

All authors made a significant contribution to the work reported, whether that is in the conception, study design, execution, acquisition of data, analysis and interpretation, or in all these areas; took part in drafting, revising or critically reviewing the article; gave final approval of the version to be published; have agreed on the journal to which the article has been submitted; and agree to be accountable for all aspects of the work.

Funding

This study was sponsored by the National Natural Science Foundation of China (82074261), Pudong New Area Traditional Chinese Medicine Brand Multiplication Plan - Chronic Nephropathy (PDZY-2021-0302) and He Liqun's famous TCM studio (PDZY-2022-0703).

Disclosure

The authors declare that there are no conflicts of interest in this work.

References

1. Sundstrom J, Bodegard J, Bollmann A, et al. Prevalence, outcomes, and cost of chronic kidney disease in a contemporary population of 2.4 million patients from 11 countries: the CaReMe CKD study. *Lancet Reg Health Eur*. 2022;20:100438. doi:10.1016/j.lanepe.2022.100438
2. Collaboration GBDCKD. Global, regional, and national burden of chronic kidney disease, 1990–2017: a systematic analysis for the Global Burden of Disease Study 2017. *Lancet*. 2020;395(10225):709–733. doi:10.1016/S0140-6736(20)30045-3
3. Jadoul M, Aoun M, Masimango Imani M. The major global burden of chronic kidney disease. *Lancet Glob Health*. 2024;12(3):e342–e343. doi:10.1016/S2214-109X(24)00050-0
4. Liu Y. Renal fibrosis: new insights into the pathogenesis and therapeutics. *Kidney Int*. 2006;69(2):213–217. doi:10.1038/sj.ki.5000054
5. Djudjaj S, Boor P. Cellular and molecular mechanisms of kidney fibrosis. *Mol Aspects Med*. 2019;65:16–36. doi:10.1016/j.mam.2018.06.002
6. Yuan Q, Tang B, Zhang C. Signaling pathways of chronic kidney diseases, implications for therapeutics. *Signal Transduct Target Ther*. 2022;7(1):182. doi:10.1038/s41392-022-01036-5
7. Frak W, Dabek B, Balcerczyk-Lis M, et al. Role of uremic toxins, oxidative stress, and renal fibrosis in chronic kidney disease. *Antioxidants*. 2024;13(6):687. doi:10.3390/antiox13060687
8. Xie T, Yao L, Li X. Advance in iron metabolism, oxidative stress and cellular dysfunction in experimental and human kidney diseases. *Antioxidants*. 2024;13(6):659. doi:10.3390/antiox13060659
9. Wang J, Liu Y, Wang Y, Sun L, Cipak Gasparovic A. The cross-link between ferroptosis and kidney diseases. *Oxid Med Cell Longev*. 2021;2021(1). doi:10.1155/2021/6654887
10. Dixon SJ, Lemberg KM, Lamprecht MR, et al. Ferroptosis: an iron-dependent form of nonapoptotic cell death. *Cell*. 2012;149(5):1060–1072. doi:10.1016/j.cell.2012.03.042
11. Jiayi H, Ziyuan T, Tianhua X, et al. Copper homeostasis in chronic kidney disease and its crosstalk with ferroptosis. *Pharmacol Res*. 2024;202:107139. doi:10.1016/j.phrs.2024.107139
12. Stockwell BR. Ferroptosis turns 10: emerging mechanisms, physiological functions, and therapeutic applications. *Cell*. 2022;185(14):2401–2421. doi:10.1016/j.cell.2022.06.003
13. Hayes JD, Dinkova-Kostova AT. The Nrf2 regulatory network provides an interface between redox and intermediary metabolism. *Trends Biochem Sci*. 2014;39(4):199–218. doi:10.1016/j.tibs.2014.02.002
14. He F, Ru X, Wen T. NRF2, a transcription factor for stress response and beyond. *Int J Mol Sci*. 2020;21(13):4777. doi:10.3390/ijms21134777
15. Yamamoto M, Kensler TW, Motohashi H. The KEAP1-NRF2 system: a thiol-based sensor-effector apparatus for maintaining redox homeostasis. *Physiol Rev*. 2018;98(3):1169–1203. doi:10.1152/physrev.00023.2017
16. Seibt TM, Proneth B, Conrad M. Role of GPX4 in ferroptosis and its pharmacological implication. *Free Radic Biol Med*. 2019;133:144–152. doi:10.1016/j.freeradbiomed.2018.09.014
17. Dodson M, Castro-Portuguez R, Zhang DD. NRF2 plays a critical role in mitigating lipid peroxidation and ferroptosis. *Redox Biol*. 2019;23:101107. doi:10.1016/j.redox.2019.101107
18. Wang J, Wang Y, Liu Y, et al. Ferroptosis, a new target for treatment of renal injury and fibrosis in a 5/6 nephrectomy-induced CKD rat model. *Cell Death Discov*. 2022;8(1):127. doi:10.1038/s41420-022-00931-8
19. Cam IB, Balci-Torun F, Topuz A, Ari E, Deniz İG, Genc I. Physical and chemical properties of cow cockle seeds (Vaccaria hispanica (Mill.) Rauschert) genetic resources of Turkey. *Ind Crops Prod*. 2018;126:190–200. doi:10.1016/j.indcrop.2018.10.022
20. Xie F, Cai W, Liu Y, et al. Vaccarin attenuates the human EA.hy926 endothelial cell oxidative stress injury through inhibition of Notch signaling. *Int J Mol Med*. 2015;35(1):135–142. doi:10.3892/ijmm.2014.1977
21. Sun H, Cai W, Wang X, et al. Vaccaria hypaphorine alleviates lipopolysaccharide-induced inflammation via inactivation of NFkappaB and ERK pathways in Raw 264.7 cells. *BMC Complement Altern Med*. 2017;17(1):120. doi:10.1186/s12906-017-1635-1
22. Wu T, Ma W, Lu W, et al. Vaccarin alleviates cisplatin-induced acute kidney injury via decreasing NOX4-derived ROS. *Heliyon*. 2023;9(11):e21231. doi:10.1016/j.heliyon.2023.e21231
23. Zhu X, Meng X, Du X, et al. Vaccarin suppresses diabetic nephropathy through <>inhibiting the EGFR/ERK1/2 signaling pathway. *Acta Biochim Biophys Sin*. 2024;56:1860–1874. doi:10.3724/abbs.2024141
24. Fu W, Zhang M, Meng Y, Wang J, Sun L. Increased NPM1 inhibit ferroptosis and aggravate renal fibrosis via Nrf2 pathway in chronic kidney disease. *Biochim Biophys Acta Mol Basis Dis*. 2025;1871(1):167551. doi:10.1016/j.bbadis.2024.167551
25. Li S, Han Q, Liu C, et al. Role of ferroptosis in chronic kidney disease. *Cell Commun Signal*. 2024;22(1):113. doi:10.1186/s12964-023-01422-8
26. Liu Y, Wang J, Badr DA. Ferroptosis, a rising force against renal fibrosis. *Oxid Med Cell Longev*. 2022;2022:1–12. doi:10.1155/2022/7686956
27. Sun S, Shen J, Jiang J, Wang F, Min J. Targeting ferroptosis opens new avenues for the development of novel therapeutics. *Signal Transduct Target Ther*. 2023;8(1):372. doi:10.1038/s41392-023-01606-1
28. Xie Y, Hou W, Song X, et al. Ferroptosis: process and function. *Cell Death Differ*. 2016;23(3):369–379. doi:10.1038/cdd.2015.158
29. Song J, Wang H, Sheng J, et al. Vitexin attenuates chronic kidney disease by inhibiting renal tubular epithelial cell ferroptosis via NRF2 activation. *Mol Med*. 2023;29(1):147. doi:10.1186/s10020-023-00735-1
30. Sihvola V, Levonen A-L. Keap1 as the redox sensor of the antioxidant response. *Arch Biochem Biophys*. 2017;617:94–100. doi:10.1016/j.abb.2016.10.010
31. Cai W, Zhang Z, Huang Y, Sun H, Qiu L. Vaccarin alleviates hypertension and nephropathy in renovascular hypertensive rats. *Exp Ther Med*. 2018;15(1):924–932. doi:10.3892/etm.2017.5442
32. Martinez-Klimova E, Aparicio-Trejo OE, Tapia E, Pedraza-Chaverri J. Unilateral ureteral obstruction as a model to investigate fibrosis-attenuating treatments. *Biomolecules*. 2019;9(4):141. doi:10.3390/biom9040141
33. Chevalier RL, Forbes MS, Thornhill BA. Ureteral obstruction as a model of renal interstitial fibrosis and obstructive nephropathy. *Kidney Int*. 2009;75(11):1145–1152. doi:10.1038/ki.2009.86

34. Aranda-Rivera AK, Cruz-Gregorio A, Aparicio-Trejo OE, Ortega-Lozano AJ, Pedraza-Chaverri J. Redox signaling pathways in unilateral ureteral obstruction (UUO)-induced renal fibrosis. *Free Radic Biol Med*. 2021;172:65–81. doi:10.1016/j.freeradbiomed.2021.05.034
35. Wang H, Liu J, Fang F, et al. Losartan ameliorates renal fibrosis by inhibiting tumor necrosis factor signal pathway. *Nefrologia*. 2024;44 (2):139–149. doi:10.1016/j.nefroe.2024.04.001
36. Bakalenko N, Kuznetsova E, Malashicheva A. The complex interplay of TGF-beta and notch signaling in the pathogenesis of fibrosis. *Int J Mol Sci*. 2024;25(19):10803. doi:10.3390/ijms251910803
37. Liu H-L, Huang Z, Li Q-Z, et al. Schisandrin A alleviates renal fibrosis by inhibiting PKCβ and oxidative stress. *Phytomedicine*. 2024;126:155372. doi:10.1016/j.phymed.2024.155372
38. Zhu B, Ni Y, Gong Y, et al. Formononetin ameliorates ferroptosis-associated fibrosis in renal tubular epithelial cells and in mice with chronic kidney disease by suppressing the Smad3/ATF3/SLC7A11 signaling. *Life Sci*. 2023;315:121331. doi:10.1016/j.lfs.2022.121331
39. Li J, Cao F, Yin HL, et al. Ferroptosis: past, present and future. *Cell Death Dis*. 2020;11(2):88. doi:10.1038/s41419-020-2298-2
40. Seiler A, Schneider M, Forster H, et al. Glutathione peroxidase 4 senses and translates oxidative stress into 12/15-lipoxygenase dependent- and AIF-mediated cell death. *Cell Metab*. 2008;8(3):237–248. doi:10.1016/j.cmet.2008.07.005
41. Jin X, He R, Lin Y, et al. Shenshuaifu granule attenuates acute kidney injury by inhibiting ferroptosis mediated by p53/SLC7A11/GPX4 pathway. *Drug Des Devel Ther*. 2023;17:3363–3383. doi:10.2147/dddt.S433994
42. Li P, Chen J-M, Ge S-H, et al. Pentoxifylline protects against cerebral ischaemia-reperfusion injury through ferroptosis regulation via the Nrf2/SLC7A11/GPX4 signalling pathway. *Eur J Pharmacol*. 2024;967:176402. doi:10.1016/j.ejphar.2024.176402
43. Canning P, Sorrell FJ, Bullock AN. Structural basis of Keap1 interactions with Nrf2. *Free Radic Biol Med*. 2015;88:101–107. doi:10.1016/j.freeradbiomed.2015.05.034
44. Wang Y, Yin Y, Liu Y, et al. Notoginsenoside R1 treatment facilitated Nrf2 nuclear translocation to suppress ferroptosis via Keap1/Nrf2 signaling pathway to alleviated high-altitude myocardial injury. *Biomed Pharmacother*. 2024;175:116793. doi:10.1016/j.biopha.2024.116793